

# CO Formation in the Thermal Decomposition of CH<sub>3</sub>ONO at High Temperatures: Kinetic Modeling of the CH<sub>3</sub>O Decomposition Rate

T. K. Choudhury, Y. He, W. A. Sanders,<sup>†</sup>

Department of Chemistry, The Catholic University of America, Washington, DC 20064

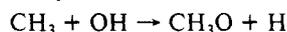
and M. C. Lin\*

Department of Chemistry, Emory University, Atlanta, Georgia 30322 (Received: May 22, 1989; In Final Form: October 16, 1989)

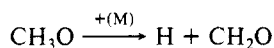
CH<sub>3</sub>ONO was pyrolyzed in two different temperature regimes in order to determine the kinetics of the CH<sub>3</sub>O decomposition reaction. A static reactor operating between 550 and 770 K was used for the first set of experiments, with analysis of products (CO, CH<sub>2</sub>O, and CH<sub>3</sub>OH) by FTIR absorption. In the second set of experiments, a shock tube operating in the range 1000–1600 K was employed and the CO product was measured by resonance absorption of the output of a stabilized CW CO laser. Kinetic modeling of CO product yields over the full range of temperature (550–1660 K) allowed us to obtain for the first time the rate constant for the decomposition of CH<sub>3</sub>O: CH<sub>3</sub>O + M → H + CH<sub>2</sub>O + M (8),  $k_8 = (5.45 \pm 0.63) \times 10^{13} \exp(-6794 \pm 102/T) \text{ cm}^3/(\text{mol}\cdot\text{s})$ , where M = Ar or He, and the error limits represent only the internal consistency of the modeled values. Theoretical implications of this result are discussed.

## Introduction

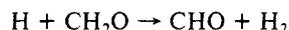
CH<sub>3</sub>O is one of the most important reactive intermediates involved in the combustion of ethers, alcohols, and hydrocarbons (saturated or unsaturated). The rapid degradation of large alkoxy and alkyl radicals formed in these systems at high temperatures ultimately produces thermochemically stable CH<sub>3</sub> radicals, which can in turn be oxidized effectively to form CH<sub>3</sub>O under combustion conditions via several processes, viz.<sup>1</sup>



In combustion media, CH<sub>3</sub>O and its decomposition product CH<sub>2</sub>O undergo fast bimolecular reactions with atoms and radicals (such as those in the examples above). This makes it difficult and unreliable to determine the rate constant for its unimolecular decomposition reaction



by kinetic modeling of flames or shock tube data. Moreover, the reverse reaction producing CH<sub>3</sub>O cannot compete kinetically with the abstraction process



Therefore, the familiar indirect method of determining the decomposition rate constant by measuring the reverse rate and applying the principle of detailed balance is also unavailable.

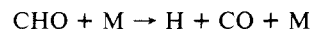
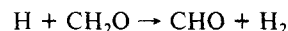
Accordingly, most combustion modeling reported in the literature has employed either "guesstimated" or calculated second-order rate constants based on the RRKM theory.<sup>1,2</sup> In view of the fact that neither the forward nor the reverse barrier for the reaction CH<sub>3</sub>O → H + CH<sub>2</sub>O is known with certainty, the results of these calculations may be unreliable. The situation would be even worse if the reverse barrier were large, since in that case the tunneling effect might be important. This is, in fact, now believed to be the case for the CH<sub>3</sub>O system.<sup>3</sup>

In order to determine the rate constant for this important unimolecular decomposition reaction, we recently carried out a series of experiments using methyl nitrite (CH<sub>3</sub>ONO) as the source of the CH<sub>3</sub>O radical. In the first of this series,<sup>4</sup> we carefully

established the kinetics and mechanism of the thermal decomposition of CH<sub>3</sub>ONO and determined the rate constants for several key processes involved in the system. These reactions, which primarily involve interactions of CH<sub>3</sub>O, NO, and HNO, are numbers 1, 3, 4, 5, and 7 in Table I.

In a subsequent experiment, CH<sub>3</sub>ONO was shock-heated in the presence of CH<sub>2</sub>O in the temperature range 1150–1700 K. Under these conditions the measured CO production rate was found to be dominated by the reaction H + CH<sub>2</sub>O → CHO + H<sub>2</sub>.<sup>5</sup> This study allowed us to determine the rate constant of the abstraction reaction reliably at temperatures relevant to combustion.

In the present study we pyrolyzed diluted CH<sub>3</sub>ONO in two different temperature regions using different heat sources and product detection methods. At the lower temperatures (550–770 K), CH<sub>3</sub>ONO was decomposed thermally in a static cell and the products were measured by an FTIR absorption technique. The decomposition products determined quantitatively were CO, CH<sub>2</sub>O, and CH<sub>3</sub>OH. In the high-temperature regime (1000–1600) K, highly diluted CH<sub>3</sub>ONO mixtures were pyrolyzed in shock waves and the major decomposition products (CO and NO) were measured by resonance absorption of CW CO laser radiation.<sup>6–10</sup> The results of our kinetic modeling and sensitivity analyses of product yields show that the overall rates of decomposition and CO production are dominated by the following reactions:



- (1) Tsang, W.; Hampson, R. F. *J. Phys. Chem. Ref. Data* **1986**, *15*, 1095.
- (2) Greenhill, P. G.; O'Grady, B. V.; Gilbert, R. G. *Aust. J. Chem.* **1986**, *39*, 1929.
- (3) Page, M.; Lin, M. C.; He, Y.; Choudhury, T. K. *J. Phys. Chem.* **1989**, *93*, 4404.
- (4) He, Y.; Sanders, W. A.; Lin, M. C. *J. Phys. Chem.* **1988**, *92*, 5474.
- (5) Choudhury, T. K.; Lin, M. C. *Combust. Sci. Technol.* **1989**, *64*, 19.
- (6) Hsu, D. S. Y.; Shaub, W. M.; Blackburn, M.; Lin, M. C. *Symp. (Int.) Combust., [Proc.]*, *19th* **1982**, 89.
- (7) Hsu, D. S. Y.; Lin, M. C. *J. Energ. Mater.* **1985**, *3*, 95.
- (8) Lin, C. Y.; Lin, M. C. *J. Phys. Chem.* **1986**, *90*, 425.
- (9) Hsu, D. S. Y.; Burks, G. L.; Beebe, M. D.; Lin, M. C. *Int. J. Chem. Kinet.* **1984**, *16*, 1139.
- (10) Hsu, D. S. Y.; Lin, M. C. *SPIE Proc.* **1984**, *482*, 79.

<sup>†</sup> Present address: Dean of Academics, U.S. Coast Guard Academy, New London, CT 06320.

\* To whom correspondence should be addressed.

The values of the kinetically modeled CH<sub>3</sub>O decomposition rate constants have been compared with those calculated by means of the RRKM theory, using the most recent ab initio potential energy surface data obtained by Page.<sup>3,13</sup> This comparison reveals that, because of the large reverse barrier (8.0 kcal/mol), H atom tunneling has a significant effect on the rate of the decomposition reaction even in the second-order region.<sup>3</sup> A more detailed discussion of the determination of this key reaction rate constant is presented below.

### Experimental Section

In the low-temperature study, a static reactor was used to pyrolyze CH<sub>3</sub>ONO-He mixtures in the temperature range 550–770 K. The experimental design of the static reactor and sample handling system has already been described in a previous publication.<sup>4</sup> The spherical Pyrex glass reaction vessel of volume 277.3 cm<sup>3</sup> was placed in a cylindrical furnace equipped with automatic temperature control. The reaction temperature was monitored by means of a thermocouple located at the center of the reactor. The reaction products were transferred directly from the reactor to a sample cell for quantitative analysis by FTIR spectroscopy. The IR cell was fitted with KCl windows.

Reaction mixtures containing 2–4% of CH<sub>3</sub>ONO in He were pyrolyzed at 24 different temperatures in the range 550–770 K at a total pressure of 710 Torr. The following absorption bands were utilized for the product analysis:

formaldehyde: 1745.7, 2782.5 cm<sup>-1</sup>

methanol: 1033.8 cm<sup>-1</sup>

carbon monoxide: 2171.2 cm<sup>-1</sup>

The accuracy of analysis was confirmed by absolute calibration, using mixtures of known composition.

In the high-temperature study, a stainless steel shock tube equipped with two frequency-stabilized CW CO lasers was used. The experimental setup has been described in previous papers by Lin and co-workers.<sup>6–10</sup> For incident shock experiments, the lengths of the driver and test sections of the shock tube are 2.5 and 4.4 m, respectively. In the present study, incident shocks were produced with reaction mixtures containing methyl nitrite and argon in the ratios 1:200.6 and 1:136.55 at temperatures from 1007 to 1666 K and at pressures between 0.6 and 1.05 atm. The temperatures and pressures of the shocked gas were calculated by the NASA/LEWIS equilibrium program in the standard way, with the shock velocity measured by BaTiO<sub>3</sub> piezoelectric gauges. He driver gas and Mylar diaphragms were used throughout the experiments. The 2 → 1 P(9) and 7 → 6 P(13) transitions of grating-tuned CW CO lasers were used to probe the concentrations of the reaction products CO and NO, respectively. The absorption signals were obtained from two InSb detectors maintained at 77 K. The detector outputs and shock timer pulses were captured

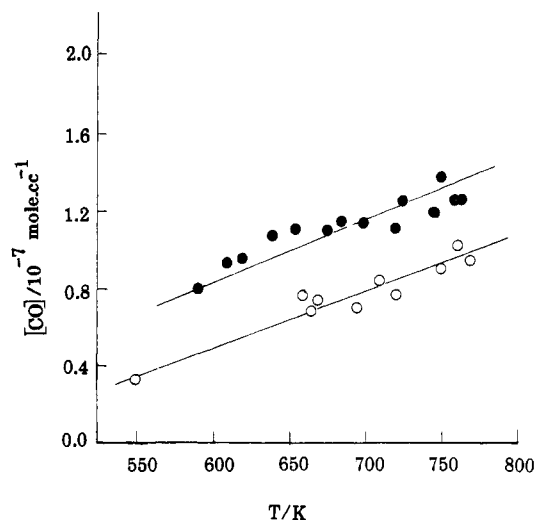


Figure 1. Concentration of CO produced in the static reactor pyrolysis at different temperatures (reaction time = 120 s, total pressure = 710 Torr). Filled and empty circles represent the results of reaction mixtures containing 2.95% and 2.25% methyl nitrite in helium, respectively. Solid lines represent the results of kinetic modeling.

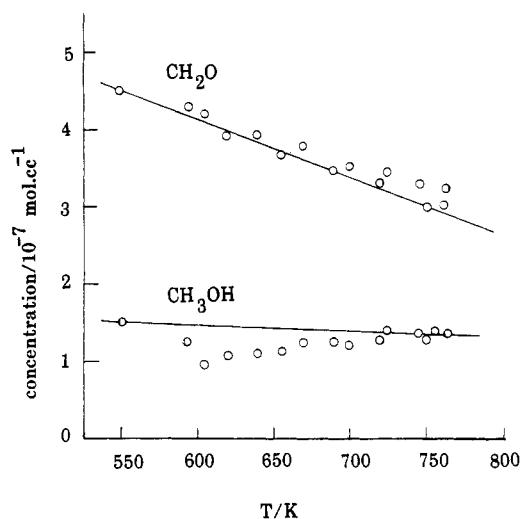


Figure 2. Concentration of CH<sub>3</sub>OH and CH<sub>2</sub>O produced in the static reactor pyrolysis of the reaction mixture containing 2.95% methyl nitrite in helium at different temperatures (reaction time = 120 s, total pressure = 710 Torr). Results of kinetic modeling are shown by the solid lines.

by three transient waveform recorders and subsequently transferred to an IBM PC. The data were then analyzed by the PC, using special algorithms for converting the detector signals to concentration profiles.

The test section of the shock tube, which has a combined leak and outgassing rate of less than  $7 \times 10^{-5}$  Torr/min (confirmed daily by overnight leak test), was diffusion pumped to  $10^{-5}$  Torr before each run. Extreme care was exercised to avoid water and oxygen contaminations in the reaction mixtures and the test section. In some of the experiments designed to test the importance of reaction 7 and its variance,  $\text{HNO} + \text{NO} \rightarrow \text{N}_2\text{O} + \text{OH}$ , H<sub>2</sub>O production was monitored with the CO laser tuned to the  $8 \rightarrow 7$  P(15) transition. No detectable amount of H<sub>2</sub>O was noted in this test. This result not only reveals the insignificance of those H<sub>2</sub>O production processes above 1000 K but also indicates the absence of H<sub>2</sub>O and/or O<sub>2</sub> impurities.

Methyl nitrite was synthesized by the procedure described in ref 4, and the prepared product was purified by repeated trap-to-trap distillations. A GC analysis of the purified methyl nitrite indicated that its purity was greater than 99.2%, with only a trace of the organic starting compound, methanol, present. Helium was supplied by Roberts Oxygen Co. and was 99.99% pure. The argon, purchased from Matheson Gas Products, was 99.9995% pure.

(11) Timonen, R. S.; Ratajczak, E.; Gutman, D.; Wagner, A. F. *J. Phys. Chem.* **1987**, *91*, 5325.

(12) Timonen, R. S.; Ratajczak, E.; Gutman, D. *J. Phys. Chem.* **1987**, *91*, 692.

(13) Page, M. To be published.

(14) Baggott, J. E.; Frey, H. M.; Lightfoot, P. D.; Walsh, R. *Chem. Phys. Lett.* **1986**, *132*, 225.

(15) Hanson, R. K.; Salimian, S. In *Survey of Rate Constants in the N/H/O System in Combustion Chemistry*; Gardiner, Jr., W. C., Ed.; Springer-Verlag: Berlin, 1984; p 361.

(16) Westley, F. *Table of Recommended Rate Constants for Chemical Reactions Occurring in Combustion*; NSRDS-NBS67; National Bureau of Standards: Washington, DC, 1980.

(17) Veyret, R.; Lesclaux, R. *J. Phys. Chem.* **1981**, *85*, 1918.

(18) Warnatz, J. In *Rate Coefficients in the C/H/O System in Combustion Chemistry*; Gardiner, Jr., W. C., Ed.; Springer-Verlag: Berlin, 1984; p 197.

(19) Tsang, W. *J. Phys. Chem. Ref. Data* **1987**, *16*, 471.

(20) Lin, C. Y.; Lin, M. C. *Combust. Sci. Technol.*, submitted for publication.

(21) Choudhury, T. K.; Sanders, W. A.; Lin, M. C. *J. Phys. Chem.* **1989**, *93*, 5143.

(22) Baggott, J. E.; Frey, H. M.; Lightfoot, P. D.; Walsh, R. *J. Phys. Chem.* **1987**, *91*, 3386. Assuming 54% of the reaction occurs by disproportionation (see ref 21).

(23) Roth, P.; Just, T. *Symp. (Int.) Combust. [Proc.]*, **20th** **1984**, 807.

**TABLE I: Reactions and Rate Constants Used in the Modeling of CO Formed in the CH<sub>3</sub>ONO System<sup>a</sup>**

| reaction  | A                     | B     | E     | ref |
|---|-----------------------|-------|-------|-----|
| 1. CH <sub>3</sub> ONO → CH <sub>3</sub> O + NO                                   | $k_1 = (0.6-3.8)E+07$ |       |       | b   |
| 2. CH <sub>3</sub> ONO → CH <sub>2</sub> O + HNO                                  | $k_2 = (0.5-5.6)E+06$ |       |       | b   |
| 3. CH <sub>3</sub> O + NO → CH <sub>3</sub> ONO                                   | $k_3 = (0.4-1.4)E+12$ |       |       | b   |
| 4. CH <sub>3</sub> O + NO → CH <sub>2</sub> O + HNO                               | $k_4 = (0.8-1.8)E+12$ |       |       | b   |
| 5. CH <sub>3</sub> O + HNO → CH <sub>3</sub> OH + NO                              | 3.2E+13               | 0.0   | 0.0   | 4   |
| 6. CH <sub>3</sub> O + CH <sub>3</sub> O → CH <sub>3</sub> OH + CH <sub>2</sub> O | 7.0E+13               | 0.0   | 0.0   | 1   |
| 7. HNO + HNO → H <sub>2</sub> O + N <sub>2</sub> O                                | 8.5E+08               | 0.0   | 3.1   | 4   |
| 8. CH <sub>3</sub> O + M → CH <sub>2</sub> O + H + M                              | 3.9E+37               | -6.65 | 33.3  | c   |
| 9. H + CH <sub>2</sub> O → CHO + H <sub>2</sub>                                   | 1.2E+08               | 1.6   | 2.2   | 5   |
| 10. CHO + M → CO + H + M  | 1.9E+17               | -1.0  | 17.02 | 11  |
| 11. H + CHO → H <sub>2</sub> + CO   | 7.2E+13               | 0.0   | 0.0   | 12  |
| 12. CHO + CHO → CH <sub>2</sub> O + CO  | 4.5E+13               | 0.0   | 0.0   | 14  |
| 13. H + HNO → H <sub>2</sub> + NO   | 1.2E+13               | 0.0   | 4.0   | 15  |
| 14. CHO + HNO → CH <sub>2</sub> O + NO  | 2.0E+11               | 0.7   | 0.0   | 16  |
| 15. CHO + NO → CO + HNO   | 7.2E+11               | -0.4  | 0.0   | 17  |
| 16. H + CH <sub>3</sub> O → CH <sub>2</sub> O + H <sub>2</sub>                    | 2.0E+13               | 0.0   | 0.0   | 19  |
| 17. H + NO + M → HNO + M  | 5.0E+15               | 0.0   | -0.6  | 16  |
| 18. HNO + M → H + NO + M  | 1.8E+16               | 0.0   | 48.7  | 15  |
| 19. H + CH <sub>3</sub> OH → CH <sub>2</sub> OH + H <sub>2</sub>                  | 3.2E+08               | 1.49  | 4.25  | 20  |
| 20. CH <sub>2</sub> OH + M → CH <sub>2</sub> O + H + M                            | 4.5E+25               | -2.5  | 34.2  | 19  |
| 21. CH <sub>3</sub> + CH <sub>3</sub> → C <sub>2</sub> H <sub>6</sub>             | 1.0E+15               | -0.6  | 0.0   | 1   |
| 22. CH <sub>2</sub> OH + NO → CH <sub>2</sub> O + HNO                             |                       |       |       | d   |
| 23. CH <sub>3</sub> + CH <sub>2</sub> O → CH <sub>4</sub> + CHO                   | 1.0E+15               | 0.0   | 22.9  | 21  |
| 24. CH <sub>3</sub> O + H → CH <sub>3</sub> + OH                                  | 2.0E+13               | 0.0   | 0.0   | e   |
| 26. CH <sub>3</sub> + CHO → CH <sub>4</sub> + CO                                  | 4.2E+13               | 0.0   | 0.0   | 22  |
| 27. OH + CH <sub>2</sub> O → H <sub>2</sub> O + CHO                               | 3.4E+09               | 1.2   | -0.4  | f   |
| 28. OH + CH <sub>3</sub> OH → CH <sub>3</sub> O + H <sub>2</sub> O                |                       |       |       | f   |
| 29. OH + CH <sub>3</sub> OH → CH <sub>2</sub> OH + H <sub>2</sub> O               |                       |       |       | f   |
| 30. H + CH <sub>2</sub> OH → CH <sub>3</sub> O + H <sub>2</sub>                   | 4.2E+06               | 2.1   | 4.9   | 19  |
| 31. OH + CHO → CO + H <sub>2</sub> O  | 3.0E+13               | 0.0   | 0.0   | 1   |
| 32. H + CH <sub>2</sub> OH → CH <sub>2</sub> O + H <sub>2</sub>                   | 6.0E+12               | 0.0   | 0.0   | 19  |
| 33. CH <sub>3</sub> + HNO → CH <sub>4</sub> + NO                                  | 4.6E+11               | 0.5   | 0.0   | 16  |
| 34. CH <sub>2</sub> O + M → CHO + H + M   | 2.0E+16               | 0.0   | 80.2  | 23  |
| 35. CH <sub>2</sub> O + M → CO + H + M  | 8.2E+15               | 0.0   | 69.5  | 23  |

<sup>a</sup>The parameters correspond to the functional form  $k = AT^B \exp(-E/RT)$ ;  $E$  is in kcal/mol, and bimolecular rate constants are in  $\text{cm}^3/(\text{mol}\cdot\text{s})$ .

<sup>b</sup>The rate constants were obtained from RRKM calculations using the parameters from ref 4. <sup>c</sup>Starting value for modeling; see text for the finalized value. <sup>d</sup>Assumed to be the same as reaction 3. <sup>e</sup>Assumed to be the same as  $\text{H} + \text{CH}_2\text{OH}$  (ref 20), which is not important in the present system. <sup>f</sup>The rate constant was calculated for each temperature by using expressions given in ref 19.

Both diluents were used without further purification.

## Results

**Low-Temperature Static Cell Experiments.** Three products (CO, CH<sub>2</sub>O, and CH<sub>3</sub>OH) were quantitatively measured by FTIR absorption spectroscopy, as described previously.<sup>4</sup> Product yields obtained as functions of temperature at a constant total pressure of 710 Torr and a fixed reaction time of 120 s are summarized in Figures 1 and 2. The yield of CO is seen to increase significantly as the temperature increases. This clearly occurs at the expense of CH<sub>2</sub>O, which appears in smaller amounts at higher temperatures. The yield of CH<sub>3</sub>OH, which is more stable than CH<sub>2</sub>O, remains essentially unchanged. As expected, the CO yield also depends strongly on the initial concentration of CH<sub>3</sub>ONO. This is illustrated by the results shown in Figure 1 for 2.25% and 2.95% CH<sub>3</sub>ONO-He mixtures.

The measured CO, CH<sub>2</sub>O, and CH<sub>3</sub>OH product yields and their temperature dependence could be accounted for quite satisfactorily by the mechanism and associated rate constants summarized in Table I. The kinetics and mechanism of this reaction system will be discussed further in the following section.

**High-Temperature Shock Tube Experiments.** Two different CH<sub>3</sub>ONO-Ar mixtures (0.728% and 0.496%) were pyrolyzed in incident shock waves at temperatures from 1000 to 1660 K and pressures from 0.6 to 1.05 atm. Typical CO concentration profiles measured by CW CO laser resonance absorption are shown in Figures 3 and 4 for the two different mixtures shocked at various temperatures. A total of 34 runs were recorded. All of the measured CO production profiles could be modeled quantitatively, as illustrated by the solid curves in Figures 3 and 4, provided the rate constant for the decomposition of the CH<sub>3</sub>O radical ( $k_8$ ) was

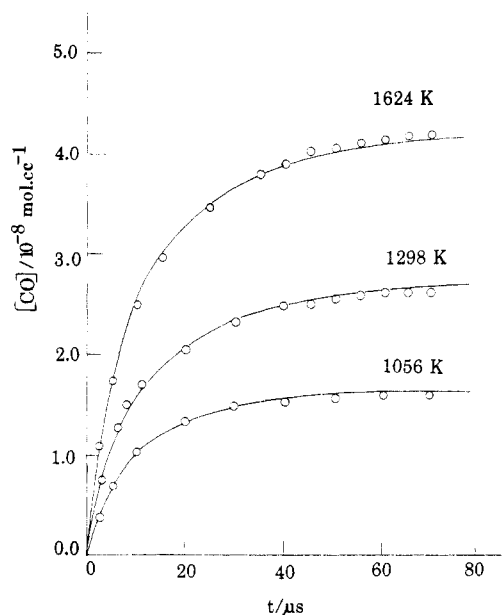


**Figure 3.** Kinetically modeled results (solid curves) and CO concentration-time profile data (circles) obtained by shocking a CH<sub>3</sub>ONO-Ar mixture in the ratio 1:136.4 at three different temperatures.

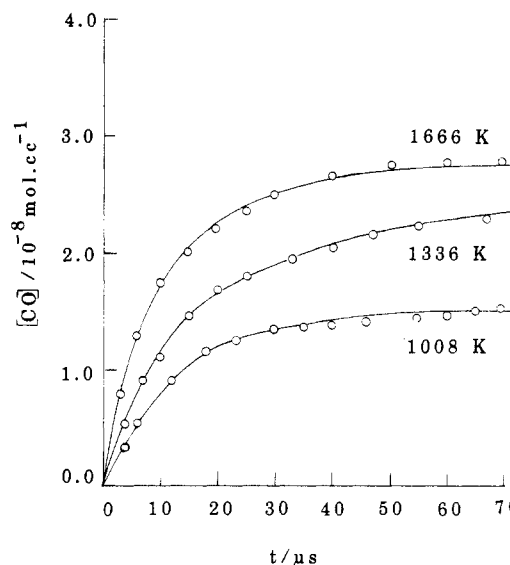


**Figure 4.** Kinetically modeled results (solid curves) and CO concentration-time profile data (circles) obtained by shocking a CH<sub>3</sub>ONO-Ar mixture in the ratio 1:200.6 at three different temperatures.

adjusted appropriately. NO was also measured in some of the runs, but the constancy of its yield as a function of time (due to its low reactivity in this temperature range) rendered the results useless for the kinetic analysis.

## Discussion

A reaction mechanism consisting of 20 species and 35 elementary reactions, summarized in Table I, was employed to interpret the measured product yields in both low- and high-temperature experiments as described in the preceding section. This mechanism, which included initially as many as 50 reactions and was subsequently reduced to 35 according to sensitivity tests, is an expanded version of the one established previously for the low-temperature (450–520 K) decomposition of CH<sub>3</sub>ONO. The new channels added include decompositions and subsequent reactions of numerous species (CHO, HNO, CH<sub>2</sub>O, and others) that become significant at higher temperatures. With the exception of a few reactions like (1)–(4), which are strongly temperature- and pressure-dependent, all of the rate constants were taken to have the values recommended in the literature (see

TABLE II: Values of  $k_8$  Obtained from Static Reactor Experiments and Kinetic Modeling of the Reaction CH<sub>3</sub>O + M<sup>a</sup>

| run | T/K   | $k_8/10^8$<br>cm <sup>3</sup> /(mol·s) | run | T/K   | $k_8/10^8$<br>cm <sup>3</sup> /(mol·s) |
|-----|-------|--|-----|-------|--|
| 1   | 550.5 | 1.2                                    | 13  | 702.5 | 44.0                                   |
| 2   | 590.5 | 7.0                                    | 14  | 708.9 | 30.0                                   |
| 3   | 607.5 | 13.0                                   | 15  | 722.5 | 44.0                                   |
| 4   | 617.0 | 16.0                                   | 16  | 726.2 | 32.0                                   |
| 5   | 643.0 | 22.0                                   | 17  | 727.5 | 47.0                                   |
| 6   | 655.5 | 28.0                                   | 18  | 748.5 | 57.0                                   |
| 7   | 660.5 | 15.0                                   | 19  | 750.5 | 58.0                                   |
| 8   | 663.0 | 15.0                                   | 20  | 751.4 | 44.0                                   |
| 9   | 667.0 | 17.0                                   | 21  | 761.5 | 67.0                                   |
| 10  | 673.5 | 31.0                                   | 22  | 761.8 | 50.0                                   |
| 11  | 689.5 | 34.0                                   | 23  | 765.5 | 72.0                                   |
| 12  | 695.0 | 24.0                                   | 24  | 771.5 | 54.0                                   |

<sup>a</sup>All the runs were carried out at 710-Torr pressure using He as diluent.

references cited in Table I). The values of the rate constants for reactions 1–4 were calculated individually for each run on the basis of the RRKM theory, using the transition-state parameters obtained by fitting our lower temperature data.<sup>4</sup> These reactions (except 4) have only minor influence on the measured CO yield, particularly under the conditions of shock tube experiments (as shown by the results of a sensitivity test to be described below).

Figures 1–4 show that the CO, CH<sub>2</sub>O, and CH<sub>3</sub>OH yields in the low-temperature (550–770 K) study, plus all of the CO production profiles obtained from the shock tube experiments (1000–1660 K), could be accounted for quantitatively, provided that the rate constant for the CH<sub>3</sub>O decomposition reaction



was appropriately increased from the value recommended by Tsang and Hampson:<sup>1</sup>

$$k_8 = 3.9 \times 10^{37} T^{-6.65} \exp(-16740/T) \text{ cm}^3/(\text{mol}\cdot\text{s})$$

The magnitude of the increase was found to be much larger at lower temperatures (e.g., a factor of ~150 at 555 K compared to ~2 at 1250 K). Our modeled values of  $k_8$  are summarized in Tables II and III as well as in Figure 5, which presents all of the data in Arrhenius form. Least-squares analyses of these data with two different functional forms give the following expressions for the rate constant over the full temperature range (550–1660 K):

$$k_8 = (5.45 \pm 0.63) \times 10^{13} \exp(-6794 \pm 102/T) \text{ cm}^3/(\text{mol}\cdot\text{s})$$

or

$$k_8 = 1.4 \times 10^{14} T^{-0.12} \exp(-6910/T) \text{ cm}^3/(\text{mol}\cdot\text{s})$$

These analyses were made with the assumption that Ar and He have approximately the same effective collision efficiency in the respective region of the temperature studied, as has been shown previously<sup>3</sup> (also see Figure 5).

To test the effects of individual rate constant variations on the measured CO yields, we carried out a series of sensitivity analyses. These consisted of doubling and halving the value of each rate constant, recomputing the yield of CO, and comparing the results with the original value in each case. Those reactions which can either increase or decrease the CO yield by more than 1% under these conditions are listed in Table IV. The six reactions to which the computed CO yields are most sensitive are, in descending order of importance, (8), (9), (10), (6), (4), and (11). The rate constants  $k_4$ ,  $k_9$ ,  $k_{10}$ , and  $k_{11}$  have been measured recently and are believed to be reliable. The rate constant  $k_6$  is perhaps least accurately known, and hence its uncertainty could affect the accuracy of  $k_8$  to some extent. However, the apparent good agreement between the static cell and shock tube data over such a wide range of conditions suggests that the values of  $k_8$  derived from the present modeling are reliable.

The effect of  $k_8$  on CO yields under static cell and shock tube conditions is demonstrated in Figures 6 and 7. The fact that the

TABLE III: Data from Shock Tube Experiments and Modeled Rate Constants for Reaction 8

| run | mixture <sup>a</sup> | T/K    | P/atm | $k_8/10^{11}$<br>cm <sup>3</sup> /(mol·s) |
|-----|----------------------|--------|-------|---|
| 1   | A                    | 1056.0 | 0.58  | 1.8                                       |
| 2   | A                    | 1085.4 | 0.81  | 1.8                                       |
| 3   | A                    | 1108.4 | 0.77  | 1.9                                       |
| 4   | A                    | 1114.6 | 0.78  | 2.2                                       |
| 5   | A                    | 1123.3 | 0.71  | 2.0                                       |
| 6   | A                    | 1235.1 | 0.79  | 3.5                                       |
| 7   | A                    | 1239.7 | 0.82  | 2.6                                       |
| 8   | A                    | 1245.6 | 0.82  | 2.7                                       |
| 9   | A                    | 1248.8 | 0.73  | 2.4                                       |
| 10  | A                    | 1297.8 | 0.77  | 2.9                                       |
| 11  | A                    | 1310.7 | 0.75  | 3.3                                       |
| 12  | A                    | 1339.2 | 0.75  | 4.0                                       |
| 13  | A                    | 1430.7 | 0.60  | 4.0                                       |
| 14  | A                    | 1458.6 | 0.83  | 6.0                                       |
| 15  | A                    | 1527.5 | 0.62  | 7.8                                       |
| 16  | A                    | 1577.8 | 0.60  | 8.0                                       |
| 17  | A                    | 1579.4 | 0.55  | 7.2                                       |
| 18  | A                    | 1624.0 | 0.81  | 8.0                                       |
| 19  | B                    | 1007.9 | 0.79  | 0.7                                       |
| 20  | B                    | 1034.9 | 0.78  | 0.7                                       |
| 21  | B                    | 1040.5 | 0.81  | 0.9                                       |
| 22  | B                    | 1068.0 | 0.80  | 1.3                                       |
| 23  | B                    | 1143.4 | 0.79  | 1.7                                       |
| 24  | B                    | 1182.0 | 0.88  | 1.9                                       |
| 25  | B                    | 1207.6 | 0.78  | 2.8                                       |
| 26  | B                    | 1275.3 | 0.74  | 2.2                                       |
| 27  | B                    | 1307.7 | 0.72  | 2.4                                       |
| 28  | B                    | 1335.9 | 0.72  | 3.6                                       |
| 29  | B                    | 1448.6 | 0.78  | 5.3                                       |
| 30  | B                    | 1480.9 | 0.87  | 5.3                                       |
| 31  | B                    | 1546.7 | 0.79  | 6.5                                       |
| 32  | B                    | 1566.2 | 0.83  | 8.0                                       |
| 33  | B                    | 1592.0 | 0.78  | 8.0                                       |
| 34  | B                    | 1666.4 | 0.79  | 8.0                                       |

<sup>a</sup>For mixture A, the ratio of methyl nitrite and argon is 1:136.55. For mixture B, the ratio of methyl nitrite and argon is 1:200.6.

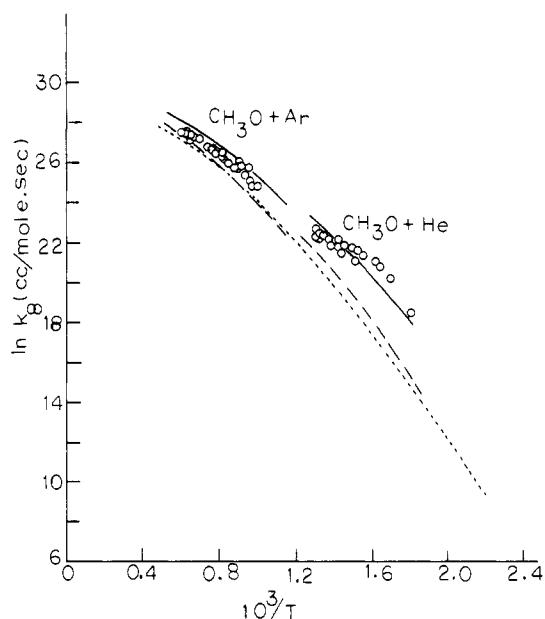


Figure 5. Comparison of theoretical and experimental values of the second-order rate constant for the methoxy radical decomposition reaction. The points are experimental data. The solid and long dashed curves are RRRM results assuming weak collisions (ref 3), with and without the tunneling correction, respectively. The dotted curve is the recommended value of Tsang and Hampson.<sup>1</sup>

effect is quite significant when the value of  $k_8$  is doubled or halved supports the validity and sensitivity of the present determination. The effect was found to be greater at lower temperatures, as one would expect because of the shorter chain length.

**TABLE IV: Results of Sensitivity Test for Elementary Reactions in the Modeling of the CH<sub>3</sub>O + M Reaction<sup>a-c</sup>**

| reaction  | % [CO] change |     |     |     |
|---|---------------|-----|-----|-----|
|   | ST            |     | SR  |     |
|   | 2k            | k/2 | 2k  | k/2 |
| 1. CH <sub>3</sub> ONO → CH <sub>3</sub> O + NO                                   | +1            | -3  | +3  | -2  |
| 2. CH <sub>3</sub> ONO → CH <sub>2</sub> O + HNO                                  | -10           | +4  | -9  | +5  |
| 3. CH <sub>3</sub> O + NO → CH <sub>3</sub> ONO                                   |               |     | -2  | +1  |
| 4. CH <sub>3</sub> O + NO → CH <sub>2</sub> O + HNO                               | -18           | +16 | -32 | +35 |
| 6. CH <sub>3</sub> O + CH <sub>3</sub> O → CH <sub>3</sub> OH + CH <sub>2</sub> O | -18           | +16 | -13 | +11 |
| 8. CH <sub>3</sub> O + M → CH <sub>2</sub> O + H + M                              | +30           | -32 | +60 | -40 |
| 9. H + CH <sub>2</sub> O → CHO + H <sub>2</sub>                                   | +20           | -21 | +8  | -9  |
| 10. CHO + M → CO + H + M  | +23           | -22 | +5  | -2  |
| 11. H + CHO → H <sub>2</sub> + CO   | -15           | +15 | -3  | +2  |
| 13. H + HNO → H <sub>2</sub> + NO   | -4            | +2  | -3  | +1  |
| 14. CHO + HNO → CH <sub>2</sub> O + NO  | -7            | +4  | -10 | +6  |
| 15. CHO + NO → CO + HNO   | -2            | +1  | +6  | 8   |

<sup>a</sup>ST: shock tube;  $T = 1297.8$  K,  $P = 0.773$  atm,  $[\text{CH}_3\text{ONO}] = 5.27 \times 10^{-8}$  mol/cm<sup>3</sup> and  $[\text{Ar}] = 7.20 \times 10^{-6}$  mol/cm<sup>3</sup>;  $t = 20$   $\mu\text{s}$ . <sup>b</sup>SR: static reactor;  $T = 750$  K,  $P = 0.934$  atm,  $[\text{CH}_3\text{ONO}] = 5.25 \times 10^{-7}$  mol/cm<sup>3</sup>;  $t = 120$  s. <sup>c</sup>Only the reactions for which changing the rate constants by a factor of 2 changes the CO concentration by 1% or more are shown in the table.

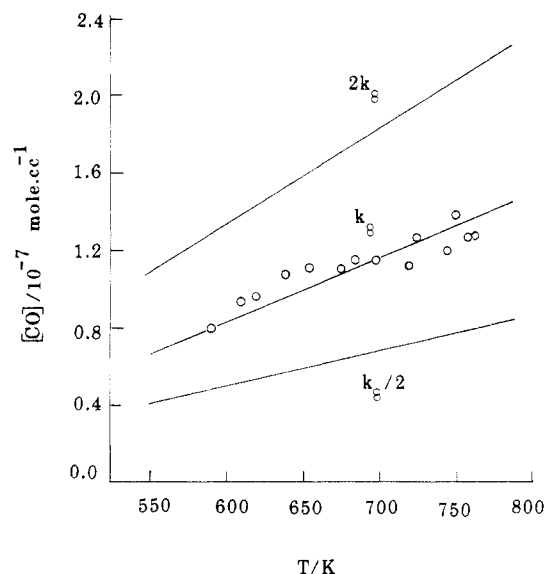


**Figure 6.** A sensitivity test for  $k_8$  in the low-temperature region. The curve in the middle at each temperature shows the results of kinetic modeling, and the circles are the results of static reactor experiments. The curves above and below show the effect of increasing and decreasing  $k_8$  by a factor of 2.

In Figure 5 we have also compared the modeled values with those predicted by the RRKM theory with and without corrections for quantum mechanical tunneling<sup>3</sup> represented by the solid and dashed curves, respectively. The tunneling correction was computed recently by Page and co-workers,<sup>3</sup> based on the method of Miller<sup>24</sup> and Garrett and Truhlar,<sup>25</sup> using a detailed set of ab initio potential energy surface data he had obtained for the CH<sub>3</sub>O → CH<sub>2</sub>O + H system.<sup>13</sup> The improved agreement between the experimental data and the theoretical curves with the tunneling correction seems to indicate that for a unique reaction like the CH<sub>3</sub>O decomposition, which involves the ejection of a hydrogen

(24) Miller, W. H. *J. Am. Chem. Soc.* **1979**, *101*, 6810.

(25) Garrett, B. C.; Truhlar, D. G. *J. Phys. Chem.* **1979**, *79*, 1079.

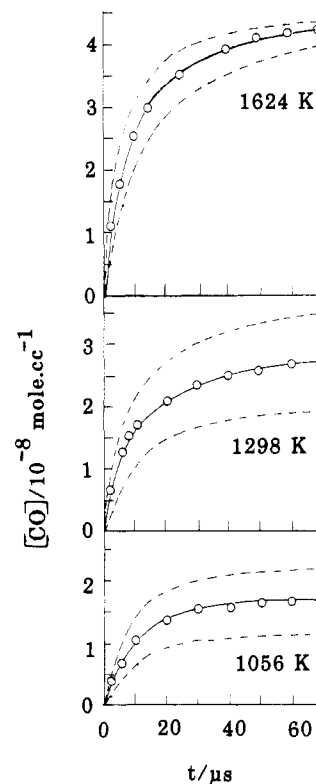


**Figure 7.** A sensitivity test for  $k_8$  in the high-temperature region. The effect of increasing and decreasing  $k_8$  by a factor of 2 on CO formation in the shock tube experiments is demonstrated with the results obtained for three different temperatures using the mixture A.

atom with a large reverse barrier (8 kcal/mol), the tunneling effect may be quite important in the second-order, pressure-dependent region. This effect was in fact found to be more pronounced at lower than high pressures as illustrated by the results summarized in Figure 2 of ref 3. This is not a surprising conclusion, since tunneling effectively lowers the reaction bottleneck and thus increases the population of the molecules that can reach the reaction threshold. The extent of the effect depends on the reverse barrier height and the nature of the transition state involved. It is worth noting that our RRKM curves with no tunneling correction shown in Figure 5 agree closely with that computed by Tsang,<sup>1</sup> who used the forward reaction barrier of 27.5 kcal/mol recommended by Batt.<sup>26</sup> This agreement is fortuitous, of course, because the linear correlation between the activation energy of decomposition and the bond dissociation energy established by Batt for larger alkoxy radicals<sup>26</sup> would not be applicable to CH<sub>3</sub>O due to the presence of the tunneling effect. In other words, the high-pressure activation energy for the unimolecular decomposition reaction of the radical is expected to be less than 25.6 kcal/mol<sup>13</sup> because of the tunneling effect.

*Acknowledgment.* We acknowledge the U.S. Department of Energy, Office of Basic Energy Sciences, Division of Chemical Sciences, for partial support of this work through Contract DE-FG05-85ER13373. M.C.L. also expresses his gratitude for the support provided by the Office of Naval Research to the Naval Research Laboratory, where the Shock tube experiments were originally carried out.

**Registry No.** CH<sub>3</sub>ONO, 624-91-9; CH<sub>3</sub>O, 2143-68-2; CO, 630-08-0.

(26) Batt, L. *Int. J. Chem. Kinet.* **1979**, *11*, 977.